Application of Generalized Partial Volume Estimation for Mutual Information based Registration of High Resolution SAR and Optical Imagery

Sahil Suri
German Aerospace Center (DLR), Remote Sensing Technology Institute
PO Box 1116, D-82230 Wessling, Germany.
Sahil.Suri@dlr.de

Peter Reinartz
German Aerospace Center (DLR), Remote Sensing Technology Institute
PO Box 1116, D-82230 Wessling, Germany
Peter.Reinartz@dlr.de

Abstract - ***Mutual information (MI) has proven its effectiveness for automated multimodal image registration for numerous remote sensing applications like image fusion. We analyze MI performance with respect to joint histogram bin size and the employed joint histogramming technique. The affect of generalized partial volume estimation (GPVE) utilizing B-spline kernels with different histogram bin sizes on MI performance has been thoroughly explored for registration of high resolution SAR (TerraSAR-X) and optical (IKONOS-2) satellite images. Our experiments highlight possibility of an inconsistent MI behavior with different joint histogram bin size which gets reduced with an increase in order of B-spline kernel employed in GPVE. In general, bin size reduction and/or increasing B-spline order have a smoothing affect on MI surfaces and even the lowest order B-spline with a suitable histogram bin size can achieve same pixel level accuracy as achieved by the higher order kernels more consistently.***

Keywords: high resolution satellite image registration, mutual information, bin size, generalized partial volume estimation

1 Introduction

Registration is a fundamental task in image processing and is used to align two or more images acquired at different times, from different sensors or from different view points. Thus, usually all remote sensing based applications require registration of images as an intermediate step. Depending upon the type of application, image registration may be called as multimodal, template, viewpoint or temporal registration. Mathematically, the problem of registering an input image (I) to a reference image (R) can be expressed as [1]:

$$R(x,y) = g\left(I\left(T(x,y)\right)\right) \quad (1)$$

where T is a transformation function which maps two spatial coordinates x and y, to the new spatial coordinates x' and y' (Equation 2) and g is a one dimensional (1D) intensity or radiometric interpolation function,

$$(x', y') = T(x,y) \quad (2)$$

The task of registration is to find an optimal spatial and intensity transformation such that images get aligned according to a predefined criterion. This task can be broken down into the following major components [2]:

i. Feature space: It extracts the information in images that will be used for matching them.
ii. Similarity metric: It determines the degree of match and mismatch between the images.
iii. Transformation: It defines the mapping of location of points in one image to new locations in another image.
iv. Search space and strategy: Search space is used to find the optimal transformation to align the images.

On the basis of feature space, image registration techniques can be classified into the following [3]:

i. Feature based techniques.
ii. Intensity based techniques.

Feature based techniques depend on accurate identification of features or objects that describe important landmarks, sharp edges or shapes, which however may often be difficult to extract. Alternatively, in intensity based techniques, images are registered based on a relation between pixel intensity values of two images. This makes the registration process to emphasize on feature matching rather than on their detection.

Automatic intensity based image registration is generally mapped as an optimization problem with an objective of maximizing the similarity metric function between the two images in a predefined search space. Two such similarity metrics, maximized to register SAR and optical images are cluster reward algorithm and mutual information [4]. Cluster reward algorithm involves computation of an expression based on estimated joint and individual histograms of the reference and the input images. On the other hand, mutual information involves computation of entropy values based on estimated joint histogram of input and reference image involved in the registration process. Details on cluster reward algorithm

can be found in the cited reference whereas MI has been discussed in a later section of this paper. MI also has been extensively used for registration of biomedical multi modal images [5]. The performance of both the mentioned similarity metrics depends profoundly on an accurate estimation of the joint histogram and so it might be affected by joint histogram bin size and the employed joint histogramming technique.

In the presented work, we evaluate MI performance consistency in terms of employed joint histogramming technique and histogram bin size. We present our analysis using normalized MI [6] as the similarity metric and generalized partial volume estimation as joint histogramming technique for histograms of various bin sizes [7]. Employment of generalized partial volume estimation suppresses appearance of interpolation induced artifacts. These are defined as periodic patterns noticed on plotting mutual information as a function of some geometric transformation at sub pixel level [8]. Apart from equal sample spacing of the images, noise has also been demonstrated as a reason for artifact appearance [9]. We perform all our tests with equally sample spaced images (1m resolution) and having inherent different noise types. As interpolation induced artifacts are not the main concern of the presented work we present analysis done at pixel level movement, though we depict the roughness of MI surfaces generated by different order B-spline kernels.

For mutual information based image to image registration, process turn around time, implementation memory requirements and generated MI surface smoothness gets affected by joint histogram bin size. For SAR to SAR image registration, speckle reduction and selection of an appropriate joint histogram bin size to generate smooth MI surfaces has been advocated [10]. On the basis of evaluated bilinear and partial volume histogramming techniques, presented work in [10] reported limitations of MI for SAR to SAR image registration due to inherent presence of multiplicative speckle noise. In the context of behavior and consistency, MI performance with respect to GPVE and different bin sizes has never been thoroughly examined. In line with the built background, prime objectives of the presented work may be enumerated as:

i. To evaluate performance of generalized partial volume estimation employing B-spline kernels with different support sizes for MI based registration of high resolution optical and SAR imagery.
ii. To study the affect of joint histogram bin size on MI surfaces produced by GPVE for images acquired over different land cover classes.

The following sections elucidate mutual information, generalized partial volume estimation, methodology adopted for the carried out evaluation followed by a final discussion and conclusions of the results obtained.

2. Mutual Information

Mutual information has evolved from the field of information theory. MI describes a statistical dependence between two random variables (e.g. A and B) expressed in terms of variable entropies.

$$MI(A,B) = H(A) + H(B) - H(A,B) \quad (3)$$

$$MI(A,B) = H(A) - H(A \mid B) \quad (4)$$

$$MI(A,B) = H(B) - H(B \mid A) \quad (5)$$

where H(A) and H(B) are the Shannon entropies of A and B respectively, H(A, B) is the joint entropy and H(A|B) is the conditional entropy of A given B and H(B|A) is the conditional entropy of B given A. Considering two remote sensing images to be registered as the two random variables, MI is a symmetric relation that always achieves values greater than zero. Registration of two images A and B is based on maximization of MI (A, B) (Equation 3). The marginal entropies and the joint entropy can be computed from [11],

$$H(A) = \sum_{a} -p_A(a) \log p_A(a) \quad (6)$$

$$H(B) = \sum_{b} -p_B(b) \log p_B(b) \quad (7)$$

$$H(A,B) = \sum_{a,b} -p_{A,B}(a,b) \log p_{A,B}(a,b) \quad (8)$$

Where $p_A(a)$ and $p_B(b)$ are the marginal probability mass functions and $p_{A,B}(a,b)$ is the joint probability mass function. These probability mass functions can be obtained from,

$$p_{A,B}(a,b) = \frac{h(a,b)}{\sum_{a,b} h(a,b)} \quad (9)$$

$$p_A(a) = \sum_{b} p_{A,B}(a,b) \quad (10)$$

$$p_B(b) = \sum_{a} p_{A,B}(a,b) \quad (11)$$

Where h is a joint histogram (JH) of the two images involved. It is a 2D matrix with the intensity values of one image along one axis and the intensity values of the other image along the other axis. The value *h (a, b)* is the statistic number of corresponding pairs having intensity value *a* in the first image and intensity value *b* in the second image. Thus, it can be seen from Equations (3) to (11) that the joint histogram is the only requirement for MI computation between any two images. The joint histogram bin size needs a vigilant selection as it can have significant

affect on the accuracy and speed of a MI based registration process. For example, a scene from TerraSAR-X [12] may have intensity values from the entire possible dynamic range of [0, 65535] (16 bit radiometry) and the corresponding scene from IKONOS-2 [13] may have intensity values in range [0, 2047] (11 bit radiometry). For a MI based registration in the mentioned scenario, the JH size without any intensity binning would be 65536 x 2048, leading to memory and computational issues. Generally, JH size can be taken care off by linear intensity binning technique. Work presented with 8 bit images in [14] enhanced both images linearly in the range (0 to 255) followed by division by a factor of 4 to reduce the bin size to 64. In practice, scenes from sensors having high radiometric resolution may not show a good distribution of intensity values over the whole histogram. Therefore, to avoid linear contrast enhancement and its possible influence on MI function we suggest the following intensity binning formulation:

$$DN_{new} = \text{round}\left(\frac{DN_{org}}{max\_dn} \times (bin\_size - 1)\right) \quad (12)$$

Where DN_{org} is the original intensity value, bin_size is the possible number of distinct intensity values in the new range, max_dn is the maximum intensity recorded in the original image and DN_{new} is the newly scaled digital number according to the bin size selected.

For the presented work we have employed the normalized MI implementation to reduce the sensitivity of MI on changes in overlap [6].

$$MI(A, B) = \frac{H(A) + H(B)}{H(A,B)} \quad (13)$$

3.0 Generalized Partial Volume Estimation

For optimizing the MI registration function, input image might be transformed several times over the reference image grid. However, in many cases, the transformed input image might not coincide with the target reference image grid. Therefore, an exact joint histogram may not be obtained and some approximation becomes inevitable. For joint histogram estimation, one step and two step histogramming techniques have been utilized in the past [9]. For the presented work one step joint histogramming technique namely generalized partial volume estimation (GPVE) has been used [7]. In this section we briefly describe GPVE along with the utilized interpolating kernels. Let I and R be the input and the reference image respectively and T be a transformation that is applied to input image grid points. Assuming T maps the grid point (x_i, x_j) in image I onto the point with coordinate, $(y_i + \Delta_i, y_j + \Delta_j)$ in the reference image R, where (y_i, y_j) is a grid point in R and $0 \leq \Delta_i, \Delta_j < 1$. GPVE is mathematically described as

$$h(I(x_i, x_j), R(y_i + p, y_j + q)) += f_1(p - \Delta_i) * f_2(q - \Delta_j) \quad (14)$$

In the equation above f_1 and f_2 refers to the kernel function selected, p and q specify the pixels involved in the joint histogram updating procedure depending upon the support of the selected kernel functions f_1 and f_2. Two conditions governing kernel function (same or different) selection are non negative increments to the joint histogram and the sum of the updated amount should equal to one for each corresponding pair of points (x_i, x_j) and $(y_i + \Delta_i, y_j + \Delta_j)$.

Normally, B-spline functions fits in the role of the kernel functions mentioned in Equation 14. Basis splines (B-splines) are one of the most commonly used family of spline functions. These are derived by several self convolutions of a basis rectangular function.

$$h_1(x) = \begin{cases} 1, & 0 \leq |x| < 0.5 \\ 0, & \text{elsewhere} \end{cases} \quad (15)$$

A B-spline of degree n or order n + 1 can be derived through n self convolutions of the function described in Equation 15.

$$h_N(x) = \underbrace{h_1(x) * h_1(x) * \ldots h_1(x)}_{N - 1 \text{ times}} \quad (16)$$

On selecting B-splines as kernel functions for GPVE the support of the selected B-spline decides the number of grid points that are involved in the updating procedure of the joint histogram. When an input image (I) is transformed to the reference image(R) grid by a selected transformation function (T) there can be two possibilities:

i. (Case 1) Transformed grid point of I is coincident with a grid point in R
ii. (Case 2) Transformed grid point of I is surrounded with grid points in R.

Depending upon the support of employed B-spline kernels in x and y directions different grid points get involved in joint histogram updating procedure for the two mentioned scenarios. For B-spline kernels (order 2 to 7), Table 1 tabulates the number of grid points involved in joint histogram updating procedure for the two cases. The ratio of maximum to minimum number of updated entries in the joint histogram updating procedure (max-min ratio), a factor reducing the artifacts appearance in the similarity metrics surfaces is also enlisted in Table 1. As expected, the max-min ratio tends to 1 as order of interpolating B-spline kernel increases.

Table1: B-spline kernel characteristic behavior as interpolating functions in GPVE

Order	Support	Case 1	Case 2	Ratio
Linear	3 * 3	1	4, 2	4.00
Quadratic	5 * 5	9	6, 4	2.25
Cubic	5 * 5	9	12, 16	1.78
Quartic	7 * 7	25	20, 16	1.56
Quintic	7 * 7	25	30, 36	1.44
Sextic	7 * 7	49	42,36	1.36

Including the ones mentioned in Table 1, the order 1 B-spline (Equation 15) can also be utilized as an interpolating kernel (nearest neighbor interpolation).

4.0 Dataset and Methodology

We present this analysis utilizing geo referenced high resolution SAR and optical imagery. SAR image has been procured by the recently launched German satellite TerraSAR-X and the optical imagery has been acquired by IKONOS-2 over Germering area near Munich (west).

Table 2: Details of TerraSAR-X and IKONOS-2 imagery

	TerraSAR-X	IKONOS-2
Mode	High resolution spot light (HS)	Reverse Scanning
Spectral Resolution	9.65 GHz	450 - 900 nm
Spatial Resolution	1m	1m (panchromatic)
Bits per pixel	16 bit	11 bit
Angle	Incidence Angle 50.80°	Nominal Collection Elevation: 63.51°
Date of Acquisition	25/12/07	14/10/07
Scene Extent	670500.0, 5338000.0 to 680000.0, 5329000.0	671973.37, 5336857.19 to 679100.37, 5330854.19
Processing Level	Enhanced ellipsoid corrected using a DEM	Standard geometrically corrected

TerraSAR-X offers various imaging modes in single or dual polarization including strip map, high resolution spot light, spot light and the scan SAR mode [12]. Table 2 tabulates the characteristics of TerraSAR-X and IKONOS-2 scenes used in the presented work.

For a thorough MI analysis, three land cover classes namely urban, forest and roads/fields have been selected. Subsets from full image scenes (Table 3) were extracted using UTM zone 32 co-ordinates. The selected image sub scenes are provided in compressed form for visualization in Figure 1.

Table 3: Details of the experimental datasets

	Dataset 1	Dataset 2	Dataset 3
Land cover	Roads/Fields	Urban	Forest
Size (pixel)	401 x 401	501 x 501	501 x 501
Scene Extent	677769.0, 533523.0 to 678169.0, 5335123.0	675618.0, 5334013.0 to 676118.0, 5333513.0	676820.50 5335889.0 to 677320.50 5335389.0
DN Range (SAR OPTICAL)	[0, 4262] [58, 1030]	[0, 15490] [1, 1745]	[0, 583] [87, 617]

The MI behavior has been analyzed in a simple experimental set up which identifies PAN as input and SAR as the reference image. The input image was put to a translation in x and y direction ranging from -20 to +20 pixels at an increment of 1 pixel in both the directions. MI values between the input and reference images as a function of x and y translation have been plotted. Ideally, MI should achieve maximum value in the search space at perfect alignment (0, 0), if there is no relative georeferencing error with in the images. The main motive is to study the dependence of MI behavior on GPVE and on the selected joint histogram bin size. Conducting such an experiment also gives an opportunity to highlight relative georeferencing differences between the IKONOS and TerraSAR-X datasets, if any. The details of three datasets used in the above described scenario are tabulated in Table 3.

5.0 Experiments and Observations

The experiments here allow us to visualize and analyze mutual information behavior in terms of consistency and smoothness of the surfaces generated. For the targeted analysis, following interpolating kernels for Equation 14 have been selected:

i. B-spline order 1 both x and y axis (K1)
ii. Cubic B-spline (order 4) for both x and y axis (K4)
iii. Sextic B-spline (order 7) for both x and y axis (K7)

The kernels for GPVE have been selected on the basis of support, order, ratio of maximum to minimum entries updated in JH. The characteristic behaviors of various B-spline kernels for GPVE have been tabulated in Table 1. B-spline order 4 and B-spline order 7 come under the category of one step joint histogram estimation as these directly estimate the joint histogram without resorting to the interpolation of intensity values at the transformed grid points on the reference grid. On the other hand, B-spline

order 1 kernel involves nearest neighborhood interpolation of intensity values at the transformed grid points on the reference grid before updating the joint histogram (two step joint histogram estimation). Presented analysis has been done at pixel level movement therefore eliminating the need and affects of interpolation for B-spline order 1 kernel and thus reducing it to a one step technique.

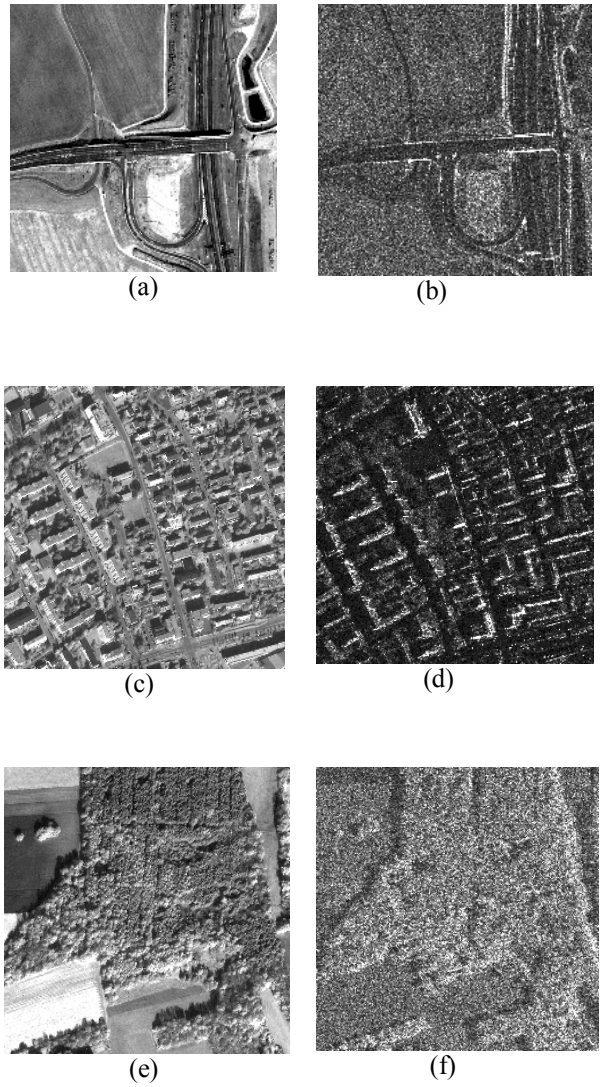

Figure 1: PAN and SAR images used in analysis. Sub figure a, c and e are the PAN images representing land cover classes roads/fields, urban and forest respectively. Sub figures b, d and f are the SAR images representing land cover classes roads/fields, urban and forest respectively.

Figure 1a, 1c, 1e courtesy of European Space Imaging © European Space Imaging

The MI performance for the three datasets namely roads/fields, urban and forests (Table 3) have been tabulated in Table 4, 5 and 6 respectively. These enlist the co-ordinates of the peak achieved by MI curve in search space of [-20, 20] pixels in x and y direction for various datasets with original and with intensities scaled to different bin sizes. The joint histogram size, defined as count of distinct intensity value pairs possible from input image (PAN) and reference image (SAR) is also provided along with. For reliable joint histogram estimation, ratio of number of image samples to the number of the joint histogram entries should be about 64 [15]. The suggested ratio has been tabulated in Table 4, 5 and 6 to visualize its affect on MI performance.

Since mutual information has proven its effectiveness as a registration similarity metric, the accuracy assessment of the peaks obtained by MI for various datasets has not been done (except for visual observation). We present a consistency analysis of MI peaks in terms of bin size and B-spline kernel selected with an assumption that the registration peak achieved by MI in most of the cases is the true registration peak for that dataset. As all the three datasets have been extracted from a single full scene it also becomes interesting to note the differences in registration peaks for the three datasets. Some differences in the registration peaks can be expected due to the very different ground conditions in the three selected areas.

In case of dataset 1 (land cover class roads/fields), for various bin size and B-spline kernel combinations MI mostly produced peak at x translation of 12 pixels and y translation of -5 pixels (Table 4). The same peak for the original intensity values and intensity values scaled down till bin size of 32 was observed for B-spline kernels 4 and 7. MI ambiguous behavior was observed for B-spline kernel 1 for original intensity values and bin size 32. As expected, MI performance became unreliable as bin size was reduced to very low values (16 and 8). The recommended ratio of image samples to joint histogram entries of around 64 did not appear as a necessary condition for this dataset as MI for the three B-spline kernels showed consistent performance for ratio ranging from 0.4 to 291.3.

Table 4: X and Y co-ordinates of peak produced by MI for land cover class roads/fields (dataset 1)

	K1	K4	K7	Size (JH)	Ratio
	15, -5	12, -5	12, -5	469x843	0.4
1024	12, -5	12, -5	12, -5	332x466	1.0
512	12, -5	12, -5	12, -5	254x209	3.0
256	12, -5	12, -5	12, -5	139x125	9.3
128	12, -5	12, -5	12, -5	78x76	27.1
64	12, -5	12, -5	12, -5	42x43	89.04
32	15, -5	12, -5	12, -5	23x24	291.3
16	0, 4	0, 4	0, 4	12x13	1030.8
8	12, 20	12, 20	12, 20	7x7	3281.7

For dataset 2 (land cover class urban), MI mostly produced peak at x translation of 12 pixels and y translation of -4 pixels (Table 5). MI showed little ambiguity for B-spline Kernel 1 with original intensity values and for bin sizes 1024, 512 and 32. Ambiguity was

also observed for B-spline kernel 4 with original intensity values but MI showed consistent peak till bin size 64 with B-spline kernel 7. Interestingly for this particular dataset, MI showed a peak very near to the original peak for bin sizes of 8. In this case, consistent MI behavior is observed for ratio ranging from 0.09 to 120.73 again exhibiting high flexibility as far as this parameter is concerned.

Table 5: X and Y co-ordinates of peak produced by MI for land cover class urban (dataset 2)

	K1	K4	K7	Size (JH)	Ratio
	18, -7	14, -5	12, -4	1270x 2057	0.09
1024	11, -4	12, -4	12, -4	807x284	1.06
512	11, -4	12, -4	12, -4	436x166	3.4
256	12, -4	12, -4	12, -4	228 x 97	11
128	12, -4	12, -4	12, -4	118 x 56	36.8
64	12, -4	12, -4	12, -4	61 x 33	120.8
32	11, -3	11, -3	11, -3	32 x 20	381.3
16	10, 6	10, 6	10, 6	16 x 13	1175
8	11, -2	11, -2	11, -2	8 x 8	3820

In case of dataset 3 (land cover class forests), MI mostly produced peak at x translation of 10 pixels and y translation of -2 pixels (Table 6). MI achieved the peak of (10, -2) for B-spline kernel 1 only with a bin size of 64 and achieved peak at (20, 17) for original intensity values and bin size of 1024. MI behavior for B-spline kernel 3 was also ambiguous with peaks varying from (20, 15) to (11, -2) and (10, -2) for various bin sizes. As order of the B-spline kernel was increased to 7, MI showed a consistent registration peak at (10, -2) for original intensity images till bin size of 32. Again, large registration errors or MI failures were recorded for very small bin sizes (16 and 8) and the image sample size and histogram entries ratio showed a high dynamic range.

Table 6: X and Y co-ordinates of peak produced by MI for land cover class forest (dataset 3)

	K1	K4	K7	Size (JH)	Ratio
	20, 17	20, 15	10, -2	408x444	1.4
1024	20, 17	20, 15	10, -2	408x444	1.4
512	20, 18	10, -2	10, -2	339x393	1.9
256	11, -2	10, -2	10, -2	175x209	6.9
128	11, -2	11, -2	10, -2	90x111	25.13
64	10, -2	11, -2	10, -2	46x57	95.73
32	11, -1	11, -2	10, -2	24x31	337.4
16	19, 11	20, 10	20,11	13x16	1207
8	20, 10	20, 11	20,11	7x8	4482

After reviewing the consistency in MI behavior for various B-spline kernels and joint histogram bin size now we turn attention towards generated MI surfaces. For brevity we show surfaces generated by the three kernels for original intensity values and intensity bin size reduced to 64 for dataset 2 (land cover class urban). To summarize, MI showed different registration peaks for the three kernels with original intensity values but on scaling the intensity values to bin size of 64 MI behavior became consistent for all the three kernels. The MI surfaces can be visualized in Figure 2-5. As clearly visible from the 2 dimensional surfaces generated B-spline order 1 generates rough MI surface using original intensity values but the smoothness and consistency of the same increases by reducing the bin size to 64. Similar behavior is depicted by B-spline order 4 though it generates much smoother MI surface as compared to B-spline order 1. As observed, B-spline order 7 generated smooth MI surfaces with a consistent behavior.

6. Discussion and Conclusions

As per expectation, application of mutual information highlighted georeferencing errors present between the examined datasets. MI gave registration coordinates at (12, -5) for land cover class roads/fields, (12, -4) for land cover class urban and (10, -2) for land cover class forests. Relative georeferencing errors of these orders were expected because of accuracy level offered by IKONOS imagery at the standard geometrically corrected level [13]. All the three datasets showed better visual overlap when the input PAN image was transformed by the obtained registration parameters.

Joint histogram bin size depending upon the joint histogramming technique may affect mutual information performance in a registration search space. The obtained results in terms of consistency and smoothness of generated MI surface clearly advocate intensity binning prior to mutual information based registration, especially for lower order B-spline kernels. Intensity binning which has an influence of a smoothing filter is also useful as it certainly reduces joint histogram sparseness and also leads to smoother mutual information surfaces very important for an optimization process. The question of best bin size selection still remains open as no fixed guidelines can be drawn from the conducted experiments. Given the limited nature of the examples, a ratio of 64 still works well, and it is possible that for other datasets this is the optimum ratio. In, other words, this ratio is not necessary for the set of data examined. As clear from observation Tables 4, 5 and 6 that ratio as low as 0.09 (Table 4) to as high as 337.37 (Table 6) can produce the same results.

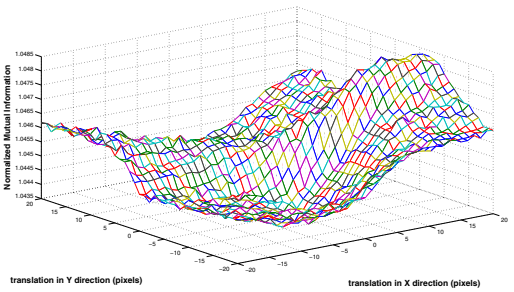

(a)

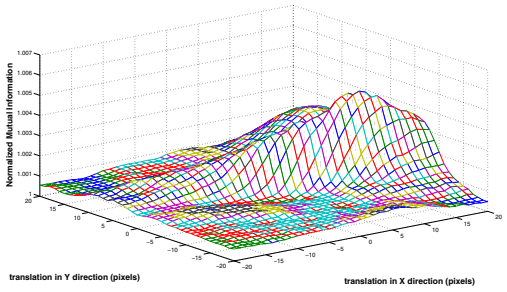

(b)

Figure 2: MI surfaces generated by B-spline order 1 kernel (a) No intensity binning, peak at (18, -7) (b) joint histogram bin size of 64, peak at (12, -4)

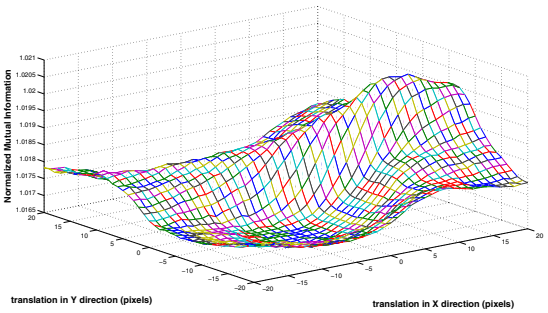

(a)

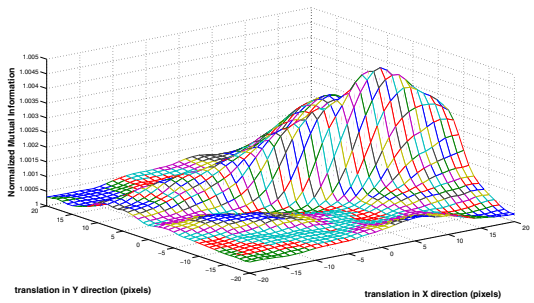

(b)

Figure 3: MI surfaces generated by cubic B-spline kernel (a) No intensity binning, peak at (14, -5) (b) joint histogram bin size of 64, peak at (12, -4)

In general, very low and very high ratio of input samples to histogram size resulting from extremely large and small bin sizes must be avoided. A very low ratio imply a sparse joint histogram and on the contrary a very high ratio may imply too many image samples updating the same histogram bin making mutual information estimate unreliable. Too small bin sizes also lead to a much smoothened image with low entropy value that might affect the mutual information performance adversely.

The generalized partial volume estimation offers a lot of flexibility in terms of available B-spline interpolating kernels for both in x and y direction. A performance of cubic B-spline and the sextic B-spline has been compared to observe that the smoothness of the MI surfaces generated increased with the support of the B-spline kernel. The B-spline order 1 kernel when limited to one step joint histogramming technique showed encouraging results as far as consistency is concerned. With a high kernel support and computational load, the sextic B-spline produced consistent results for various bin sizes selected. Though all the B-splines can be easily implemented with the help of look up Tables but still the computational load for the first order B-spline is the least.

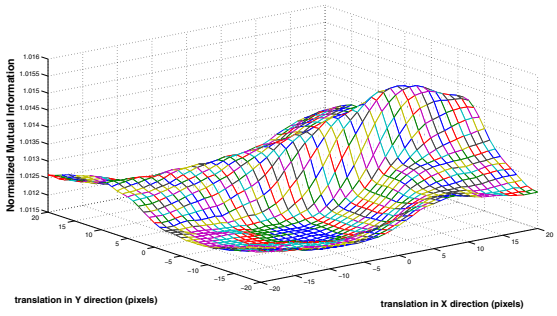

(a)

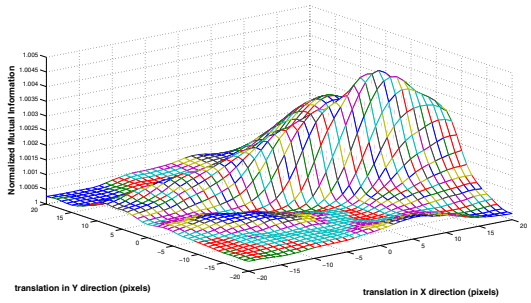

(b)

Figure 4: MI surfaces generated by sextic B-spline kernel (a) No intensity binning, peak at (12, -4) (b) joint histogram bin size of 64, peak at (12, -4)

With advancement in research and technology modern satellites like IKONOS-2 and TerraSAR-X provide already geocoded and terrain corrected data products. A useful contribution of the presented analysis is to highlight the magnitude of registration differences that might be present with in images procured from different agencies and with dissimilar accuracy levels. In an exhaustive registration parameter search, B-spline first order kernel with suitable intensity binning and pixel level movement may yield similar registration results as the higher order B-splines. If the application is limited by processing hardware then the use of first order splines

along with suitable intensity binning is appropriate, however, the higher order splines in general are more robust.

References

[1] L.G. Brown, **"**A survey of image registration techniques", *ACM Computing Surveys*, Vol. 24, No. 4, pp.325-376, 1992.

[2] B.Zitová and J. Flusser, "Image registration methods: a survey". *Image and Vision Computing*, Vol. 21, No.11, pp.977-1000, 2003

[3] H. Li, B. S. Manjunath, and S. K. Mitra, "A contour-based approach to multisensor image registration," *IEEE Transactions on Image Processing*, vol. 4, no.3, pp. 320–334, 1995.

[4] J. Inglada and A. Giros, "On the possibility of automatic multisensor image registration", *IEEE Transactions on Geoscience and Remote Sensing,* vol. 42, no. 10, pp. 2104-2120, 2004

[5] J. Pluim, J. Maintz, and M. Viergever, "Mutual Information Based Registration of Medical Images: A Survey," *IEEE Transactions on Medical Imaging*, vol. 22, no. 8, pp. 986-1004, 2003

[6] C. Studholme, D. L. G. Hill, and D. J. Hawkes, "An overlap invariant entropy measure of 3D medical image alignment," *Pattern Recognition*, vol. 32, no. 1, pp. 71–86, 1999.

[7] H. Chen and P. K. Varshney, "Mutual information-based CT-MR brain image registration using generalized partial volume joint histogram estimation," *IEEE Transactions on Medical Imaging*, vol. 22, pp. 1111-1119, 2003.

[8] J. Pluim, J. Maintz and M.Viergrever, "Interpolation artifacts in mutual information based image registration", *Computer Vision and Image Understanding,* vol. 77 pp.211-232, 2000.

[9] H. Chen and P.K. Varshney, "Mutual Information: A Similarity Measure for Intensity Based Image Registration", Chapter 3 of Advanced Image Processing Techniques for Remotely Sensed Hyperspectral Data, Editor P.K. Varshney and M.K. Arora, pp. 89-108. Publisher: Springer Verlag, 2004.

[10] H. Xie, L. E. Pierce and F. T. Ulaby, "Mutual Information based registration of SAR images", *IEEE Geoscience and Remote Sensing Symposium*, IGARSS'03 Toulouse, France 21-25 July 2003 Proc. Vol 6, pp. 4028 - 4031

[11] H. Chen, P. K. Varshney, and M. K. Arora, "Mutual information based image registration for remote sensing data." *International Journal of Remote Sensing,* Vol. 24, no. 18, pp. 3701-3706, 2003.

[12] A. Roth, "TerraSAR-X: a new perspective for scientific use of high resolution space borne SAR data" *2nd GRSS/ISPRS Joint Workshop on Remote Sensing and Data Fusion over Urban Areas*, Berlin Germany 22-23 May 2003. Proc. pp. 4-7

[13] Technical guide, IKONOS imagery
Source:
http://glcf.umiacs.umd.edu/data/guide/technical/IKONOS_Product_Guide_jan06.pdf

[14] A.A. Cole Rhodes, K.L.Johnson, J.LeMoigne and I.Zavorin "Mutualresolution registration of remote sensing imagery by optimization of mutual information usng a stochastic gradient", *IEEE transactions on image processing* vol. 12, no. 12, pp.1495-1511, 2003

[15] H.Chen and P.K.Varshney, " Size-dependent image resampling for mutual information based remote sensing image registration" *IEEE International Geosceince and Remote Sensing Symposium* Proceedings, CD-ROM, Anchorage, Alaska, Sept. 20-24, 2004.